Available online at www.sciencedirect.com

SciVerse ScienceDirect

Ceramics International 39 (2013) 5545–5552

CERAMICS INTERNATIONAL

www.elsevier.com/locate/ceramint

Electrochemical behavior and photocatalytic performance of nitrogen-doped TiO_2 nanotubes arrays powders prepared by combining anodization with solvothermal process

Zuoli He[a,b], Wenxiu Que[a,b,*], Yucheng He[a,b], Jiaxing Hu[a,b], Jing Chen[a,b], Hafiz M. Asif Javed[a,b], Yune Ji[a,b], Xiaonan Li[a,b], Duan Fei[a,b]

[a]*Electronic Materials Research Laboratory, School of Electronic and Information Engineering, Xi'an Jiaotong University, Xi'an 710049, Shaanxi, People's Republic of China*

[b]*International Center for Dielectric Research, Xi'an Jiaotong University, Xi'an 710049, Shaanxi, People's Republic of China*

Received 16 November 2012; received in revised form 17 December 2012; accepted 19 December 2012
Available online 28 December 2012

Abstract

Nitrogen-doped TiO_2 nanotubes arrays (TNAs) powders were prepared by a two-step process, which combines an anodization method with a solvothermal treatment process. Physicochemical features of the nitrogen-doped TNAs powders were characterized by X-ray diffraction analysis, scanning electron microscopy, X-ray photoelectron spectroscopy, and diffuse reflectance ultraviolet–visible spectroscopy. Electrochemical behavior and photocatalytic performance were also measured. Results indicate solvothermal treatment transforming the TNAs powder to anatase and ammonia being the nitrogen-doping source. The electrochemical properties of the TNAs show the reversible capacity of the TNAs to be good and the TNAs powders obtained after solvothermal treatment at 100 °C for 3 h to have the best photocatalytic activities among all the measured samples due to a proper crystalline.

Keywords: D. TiO_2; Photocatalyst; Nanotube; Electrochemical

1. Introduction

Titania (TiO_2) is a typical transition metal oxide semiconductor with high chemical stability, low-costs, non-toxicity, strong photocatalytic activity and high photoelectric conversion efficiency. These unique physical and chemical properties make it an excellent material for various applications, such as photocatalysts, dye-sensitized solar cells, gas sensors, electrochemical applications and many other applications [1–6]. However, the relatively large band gap of TiO_2 requires ultraviolet (UV) light for electron–hole separation, which is only 5% of the natural solar light. It is of great significance to develop photocatalysts that can be used in both UV irradiation (290–400 nm) and visible light (400–700 nm) to enhance the photocatalysis efficiency [7]. An approach is to dope TiO_2 with anions such as N, S, and F, which results in the p-states near the valence band much like other deep donor levels in semiconductors [5,7–9]. Nitrogen doping has been shown to extend the light absorption onset from 380 nm to visible light (usually above 500 nm) and to offer possible photocatalytic activity under visible light irradiation [9–12]. For photocatalysis, several physical parameters (such as crystallinity, grain size, pores and surface area) have been proven to influence its photocatalytic activity [9–13]. Hence, significant efforts have been made to synthesize TiO_2 with specifically designed meso/microporous microstructures, desired morphologies, and high crystalline framework, so as to achieve excellent transport behaviors [13–17]. As compared with other forms of nanostructured TiO_2 materials, one-dimensional nanomaterials such as nanotubes, especially electrochemical

*Corresponding author at: Electronic Materials Research Laboratory, School of Electronic and Information Engineering, Xi'an Jiaotong University, Xi'an 710049, Shaanxi, People's Republic of China.
Tel.: +86 29 82668679; fax: +86 29 82668794.
E-mail address: wxque@mail.xjtu.edu.cn (W. Que).

0272-8842/$ - see front matter
http://dx.doi.org/10.1016/j.ceramint.2012.12.068

anodized TiO_2 nanotubes, are the most attractive candidates for photocatalysis due to their strong light scattering effects and high surface-to-volume ratio. Highly ordered/vertically oriented tubular structure is very suitable for a high degree of electron mobility along the tube axis, also perpendicular to the substrate, which is greatly helpful to reduce interface recombination [12,18–24].

On the basis of the above discussions, we report synthesis of anatase nitrogen-doped TiO_2 nanotubes arrays (N-TNAs) powders through a facile combination of anodization method and solvothermal process. Higher-order and micro-sized superstructures of amorphous TNAs are formed during anodization, the solvothermal treatment transform the amorphous TNAs powders to anatase, and ammonia used in the synthesis serves as a nitrogen-doping source. So the formation of anatase and nitrogen-doping in TNAs powders can be simultaneously completed during the solvothermal process. Electrochemical behavior and photocatalytic performance are also measured and discussed. It is proposed that the TNAs electrode might have potential application in electrochemical storage, and proper crystalinity can improve photocatalytic activity by balancing the formation and recombination of the electron–hole pair.

2. Experimental section

2.1. Chemicals and materials

Titanium foils (2 × 5 cm, 99.5% purity, 0.2 mm thick) were purchased from General Research Institute for Nonferrous Metals, China. Before anodization, they were carefully cleaned by foamless eradicator and then degreased by sonication in acetone, ethanol, and de-ionized water. Ethylene glycol, ethanol, ammonium fluoride, ammonia and methyl blue are analytically pure and were purchased from Hongyan Group Chemical Reagent Co. Ltd., China.

2.2. Synthesis procedures

2.2.1. Preparation of TiO_2 nanotube arrays

TiO_2 nanotube arrays (TNAs) were synthesized on the surface of titanium foils by the anodization method. Two pieces of the Ti foils were used in the anodization process, one as the working electrode and the other as the counter electrode. Two electrodes were immersed into the electrolyte solution containing 97 vol% ethylene glycol, 0.3 wt% ammonium fluoride and 3 vol% of H_2O. The anodic oxidation was carried out at room temperature by applying a voltage of 50 V for 6 h using a DC power supply (Model GPS-3303c, GW Instrument Co. Ltd., Taiwan). Fig. 1 shows the schematic diagram of the anodization process. During the reaction process, magnetic stirring was carried out to ensure electrolyte solution uniformity. After anodization, the obtained pale yellow TNAs were washed with de-ionized water and then soaked in the ethanol for more than 8 h. Finally, dried in oven at 80 °C for another 8 h, thus the TNAs powders were finally prepared and will be used in the next step with further treatment.

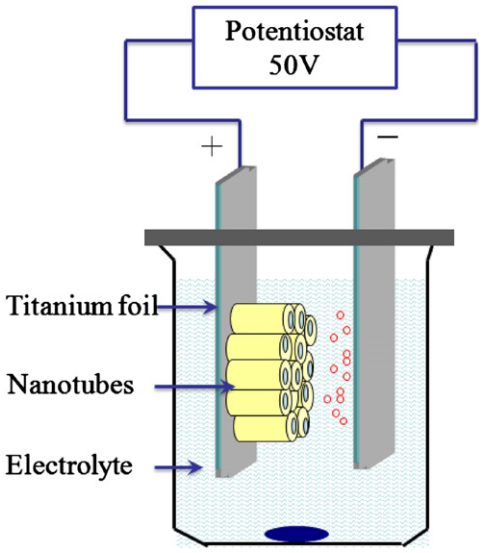

Fig. 1. Schematic diagram of the anodization processing.

2.2.2. Preparation of N-TNAs powders

Disperse a given amount of the as-prepared TiO_2 nanotube powders into solution with 20 mL ethanol, 10 mL H_2O and 0.5 mL ammonia with an assistance of strong magnetic stirring. After being stirred for about 30 min, the final mixture was directly transferred into a 50 mL teflon stainless autoclave. The autoclave was maintained in oven at 80 °C, 100 °C, 120 °C, and 150 °C for 3 h and then cooled down to room temperature. Thus, white solid powders were obtained by washing with ethanol and de-ionized water for several times, and the N-TNAs powders were finally prepared after dried in the air at 80 °C.

2.3. Characterization

Scanning electron microscopy (SEM) was used to characterize the morphological and structural properties of the TNAs and the N-TNAs powders. Crystallographic phase of the prepared samples were investigated by X-ray diffraction at room temperature, using a D/max-2400 X-ray diffraction spectrometer (Rigaku) with CuKα radiation and operated at 30 kV and 100 mA from 15° to 75°, and the scanning speed was 15° min^{-1} at the step of 0.02°. Elemental composition of the samples were determined by X-ray photoelectron spectroscopy (XPS) obtained on an Axis Ultra, Kratos (UK) using monochromatic AlKα radiation (150 W, 15 KV, 1486.6 eV). The vacuum in the spectrometer was 10^{-9} Torr. Binding energies were calibrated relative to the C1s peak (284.8 eV) from hydrocarbons absorbed on the surface of the samples. UV–vis absorption spectra of the samples were obtained by a JASCO Model V-570 UV/VIS/NIR spectrometer with a wavelength range from 300 nm to 800 nm.

2.4. Electrochemical measurements

Electrochemical properties of the TNAs electrodes were monitored in KCl saturated solution (pH ≈ 7.0) using an electrochemical workstation (CorrTestTM-CS300, Wuhan, China) [25], three electrode systems were used in the experiment with a modified glassy carbon electrode (3 mm in diameter) as the working electrode, which contains 70 wt% N-TNAs powders, 20 wt% graphite and 10 wt% paraffin, where Pt foil and Ag/AgCl electrode were used as the counter electrode and reference electrode, respectively.

2.5. Photocatalytic activity measurements

Photocatalytic activity of the prepared samples was evaluated through the degradation of 20 mg/L methyl blue (MB) in a BL-GHX-V multifunctional photochemical reactor (Shanghai Bilon Experiment Equipment Co. Ltd., Shanghai, China) under an irradiation of a medium-pressure Hg lamp (300 W). 25 mg of photocatalyst was added into 250 mL 20 mg/L MB solution and stirred for 15 min, then the solution was further dispersed by sonication and then transferred to test tubes. Stirring was performed during the

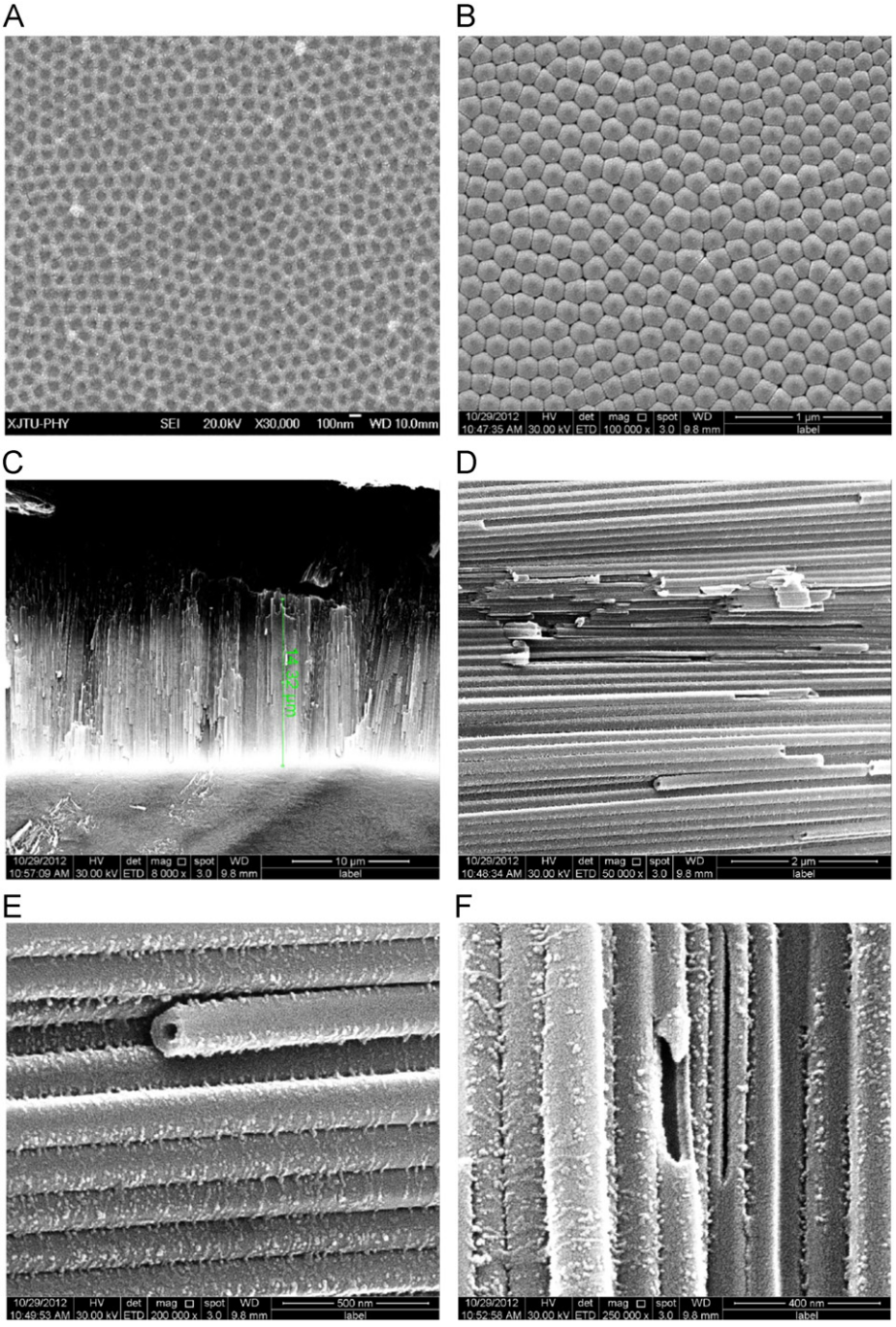

Fig. 2. SEM images of the TNAs powders prepared via solvothermal process at 150 °C for 3 h. (A) top view; (B) bottom view; (C–F): side view.

reaction. Sampling was also performed at regular intervals. Residual concentration of the MB solution was determined by measuring its absorbance at 665 nm using an UV–vis spectrophotometer (UV-2550) [26].

3. Results and discussion

3.1. SEM analysis

The diameter and length of the as-prepared TNAs can be affected by the anodization conditions, such as applied voltage, oxidation time, oxidation temperature and electrolyte. Once the DC power is supplied vigorous gas bubbles are immediately generated at the cathode, while the color of the Ti foil (as the anode) is turned into pale purple at the surface. After a few minutes, white nanotubes start to form on the Ti foil surface and the nanotube layer becomes thicker with increase in the reaction time. To analyze the morphology of the prepared TNAs after the solvothermal treatment at 150 °C for 3 h, scanning electron microscope (SEM) was carried out. As can be seen from the top view shown in Fig. 2A, higher-order and micro-sized superstructures of nanotube arrays can be easily obtained via electrochemical anodization process. It also can be observed that the top of the tubes is still open and the pores of the tubes are not very circular. The nanotube arrays are close at the bottom as seen from the bottom view in Fig. 2B, and the thickness of the nanotube layer (the length of the nanotube) is about 1400 nm as shown in Fig. 2C. After solvothermal treatment, the surface of the TNAs became rough and is covered with small nanoparticles as shown in Fig. 2E. The external diameter of the nanotube is about 50 nm, the external diameter size is about 130 nm, and the thickness of the nanotube wall is about 40 nm as shown in Fig. 2E and F.

3.2. X-ray diffraction analysis

It is well known that TiO_2 mainly exists in anatase, brookite and rutile phases. Among them, best photocatalytic activities have been found from anatase phase [6,9,10]. X-ray diffraction was employed to characterize the samples. Fig. 3 shows the XRD patterns of TiO_2 nanotube arrays before and after the solvothermal treatment. It can be seen that TNAs obtained before the solvothermal treatment only have a very weak diffraction signal of Ti toil. After the solvothermal treatment, the as-prepared TNAs show anatase characteristic diffraction peaks (JCPDS Patterns No. 21-1272, $I4_1/amd$, $a=b=3.785$ Å, $c=9.514$ Å), and the crystalline property becomes obvious with increase in the reaction temperature. The peaks at scattering angles of 25.26°, 37.88°, 47.78° and 62.66° correspond to the reflections from the (101), (004), (200) and (204) crystalline planes of anatase TiO_2, respectively [27]. These results indicate that the solvothermal process transform the amorphous TNAs to anatase.

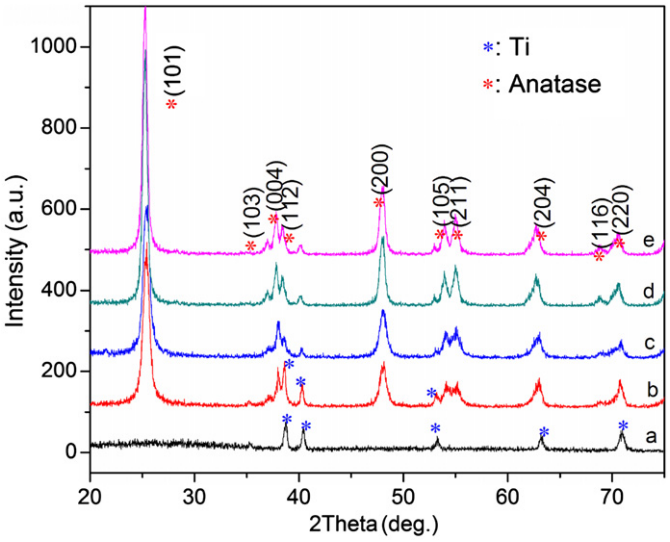

Fig. 3. XRD patterns of the TNAs powders prepared at different conditions. a, before solvothermal process; b, 80 °C for 3 h; c, 100 °C for 3 h; d, 120 °C for 3 h; and e, 150 °C for 3 h.

The reactions may occur as follows:

$$NH_3 \cdot H_2O \leftrightarrow NH_3 + H_2O \leftrightarrow NH_4^+ + OH^- \quad (1)$$

$$TiO_x + 4OH^- \rightarrow Ti(OH)_4 + x/2O_2 (1 < x \leq 2) \quad (2)$$

$$Ti(OH)_4 + 2NH_3 \rightarrow TiO_2 + 2NH_3 \cdot H_2O \quad (3)$$

Above reactions indicate that $NH_3 \cdot H_2O$ is just a catalyst in this process and plays an important part during the solvothermal process. Since the NH_3 content can increase when the reaction temperature increases, thus the crystallsation can become more obvious with an increase of the reaction temperature

3.3. XPS analysis

Chemical composition of the as-prepared TiO_2 photocatalyst sample was examined by X-ray photoelectron spectroscopy (XPS). Fig. 4 shows the XPS spectra of the TNAs powders prepared via the solvothermal process at 100 °C for 3 h, which are fitted with the nonlinear least-squares fit program using the Gauss–Lorentzian peak shapes. As shown in Fig. 4A, the N1s peak located at the region of 398 eV indicates the possible presence of nitride species (such as Ti–N) and these species may coordinate with surface of titania, which come from the ammonia in the reaction solution [6,8,9,28,29]. The O1s XPS spectrum exhibits an additional peak at 529.6 eV corresponding to the Ti–O bond (as shown Fig. 4B) [6]. Fig. 4C shows that the peak position of Ti 2p3/2 corresponds to that of the Ti^{4+} oxidation state, and the shape of the Ti2p excludes the presence of traceable amount of Ti^{4+}, which also confirms that the $NH_3 \cdot H_2O$ just acts as a catalyst during the solvothermal process.

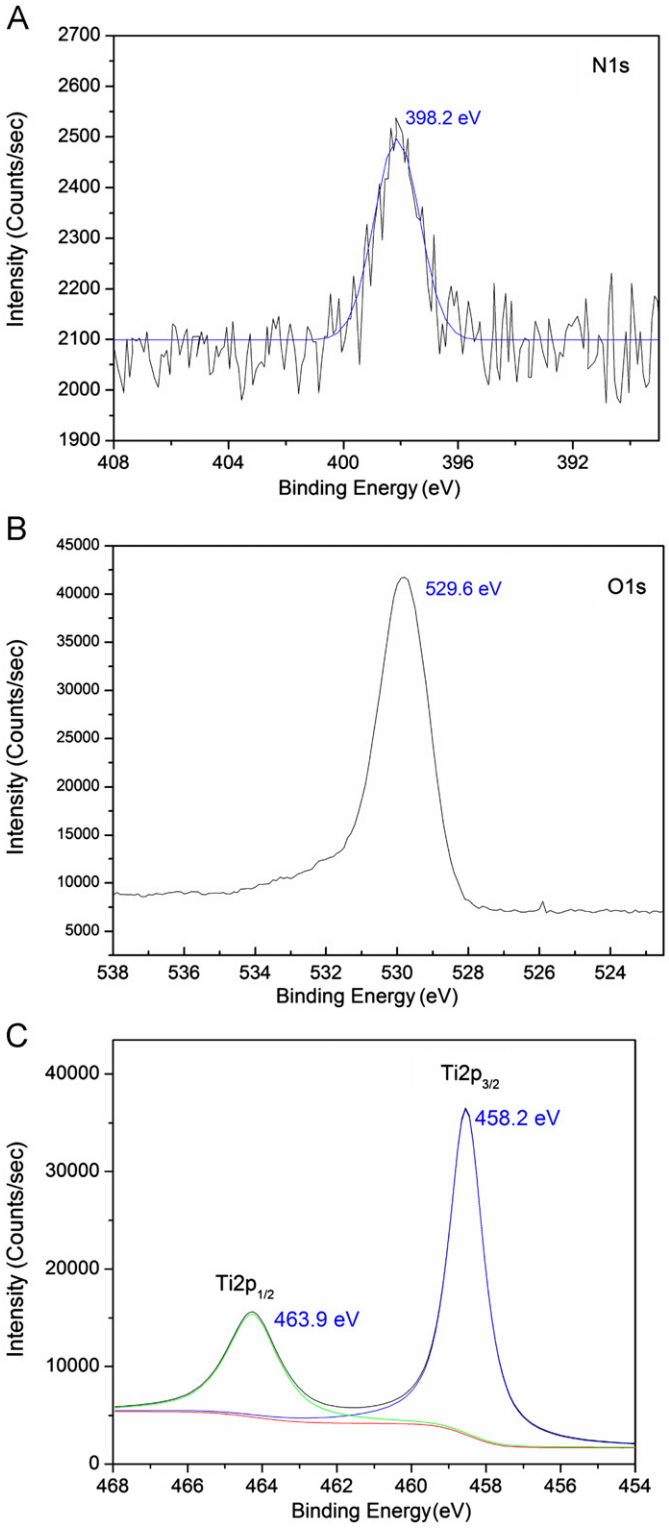

Fig. 4. (A) N1s XPS spectrum; (B) O1s XPS spectrum; and (C) Ti2p XPS spectrum of the TNAs powders prepared via solvothermal process at 150 °C for 3 h.

3.4. UV–vis absorption spectra analysis

Fig. 5 shows the UV–visible spectra of the TNAs powders in the wavelength range of 200–800 nm. It can be seen that for the TNAs before solvothermal process, the absorption spectrum is cutoff at ~375 nm. While for the TNAs after the solvothermal treatment, an add-on shoulder is imposed onto the cutoff edge of the absorption spectrum, which leads to a shift of the absorption from 380 to 390 nm. By applying Tauc's equation, the optical band gap energy (Eg) of the as-synthesized products can be calculated. Based on Tauc's formula $[(Ahv)=B(hv-Eg)^n]$, the relationship between the absorption coefficient and the incident photon energy of semiconductors can be obtained, where A is the absorption coefficient, hv is the photon energy, B is a constant and n is a value that depends on the nature of the electronic transition which is responsible for the absorption ($n=1/2$ for direct transitions and $n=2$ for indirect transitions). The inset curves in Fig. 5 exhibit the optical band gaps of the TNAs powders (obtained by extrapolation) and their values are about 3.2 eV for the TNAs powders obtained before and after solvothermal process at 80 °C for 3 h, and 3.1 eV for the other samples, respectively, which are very close to the optical band gap values as reported in the literatures [6,9]. The UV–visible absorption results indicate there is a red-shift of the optical energy gap, which may be resulted from the N-doping during the solvothermal process. Such light absorbance enhancement in the near-UV region and in the visible light range is consistent with the yellow color characteristic of the TNAs powders. That is to say, the extension of the light absorption from the UV to visible range should be ascribed to the contribution of the doped nitrogen atoms and oxygen vacancies in TiO_2 lattice, the interstitial nitrogen atoms induce the local states near the valence band edge and thus the oxygen vacancies give rise to the local states below the conduction edge. Such an excitation from the local states to the conduction band corresponds to the "add-on shoulder" of the absorption edge of the UV–visible spectrum as reported in Ref. [6].

3.5. Electrochemical performance

The CV measurement was carried out at room temperature at the scan rate of 50 mV/s in KCl saturated solution in a potential range from −0.4 V to 0.4 V, and the CV curves of the TNAs electrode are shown in Fig. 6. The potential difference between anodic and cathodic peak positions (ΔE_p) is used to estimate the reversibility of the electrode reaction. The ΔE_p value of the TNAs electrode before the solvothermal treatment is smaller than that of the TNAs electrode after solvothermal treatment after the 20th scan, which indicates that the reversibility of the redox reaction of the TNAs electrode becomes better after the solvothermal process. This could be due to the increased defects and surface area, which can increase the number of the active points in the electrode, thus the electrochemical performance can be improved. In all, the preliminary electrochemical experiment shows that the TNAs electrode might have potential application in electrochemical storage.

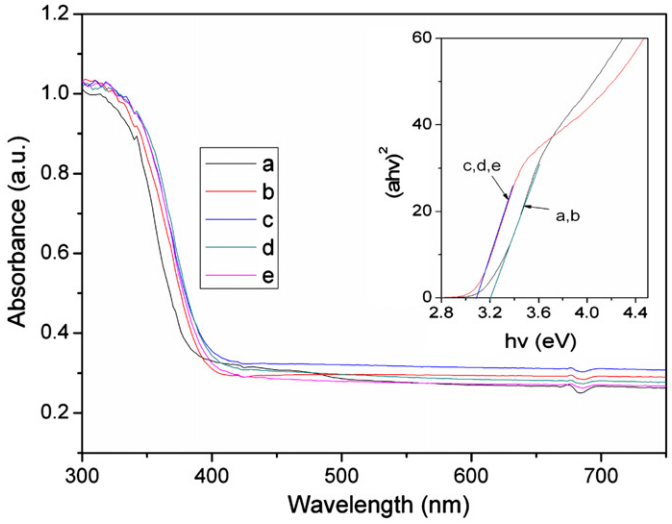

Fig. 5. UV–visible absorption spectra of the TNAs powders prepared at different conditions and the inset shows direct band gap estimation: a, before solvothermal process; b, 80 °C for 3 h; c, 100 °C for 3 h; d, 120 °C for 3 h; e, 150 °C for 3 h.

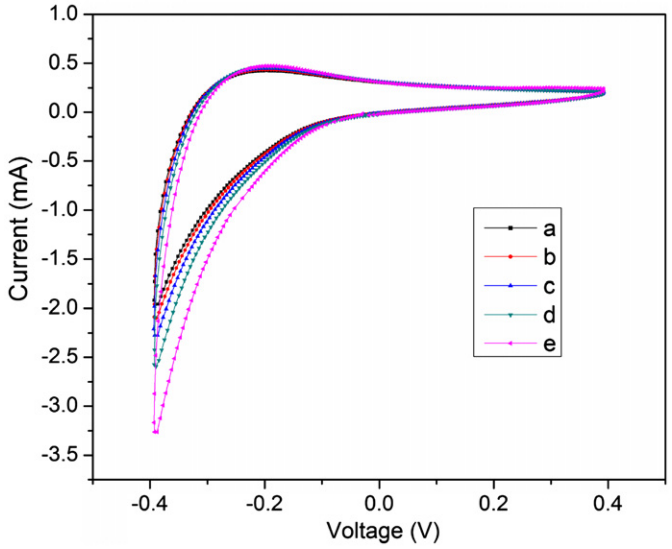

Fig. 6. CVs of the TNAs electrode after twentieth circles. a, before solvothermal process; b, 80 °C for 3 h; c, 100 °C for 3 h; d, 120 °C for 3 h; e, 150 °C for 3 h.

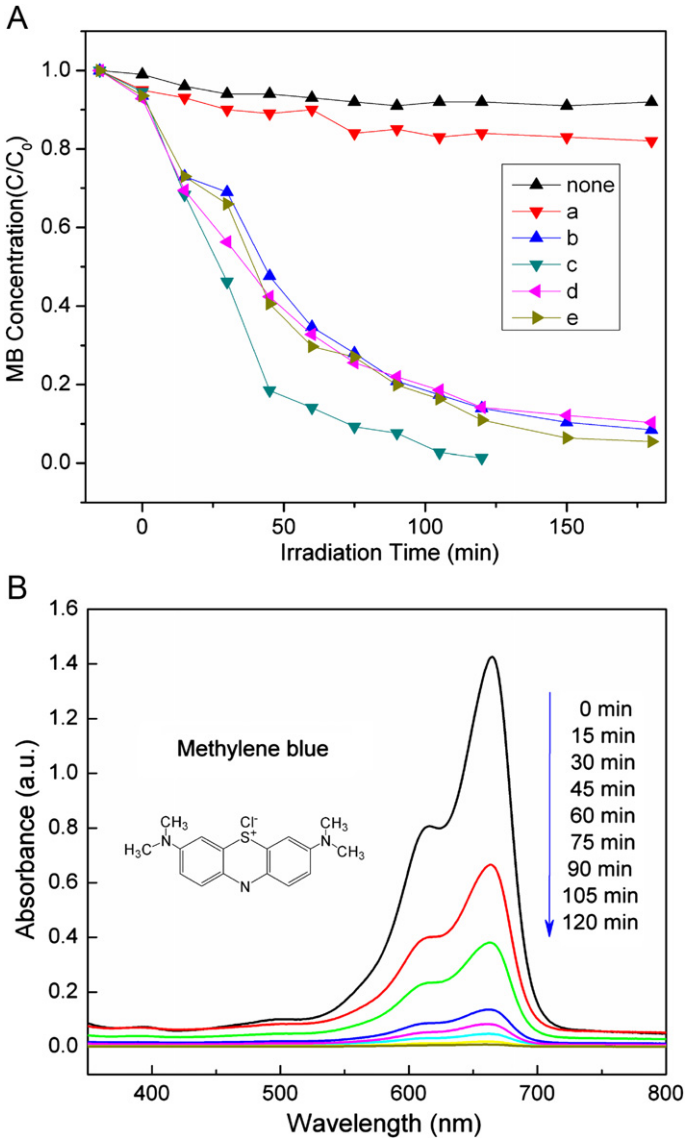

Fig. 7. (A) Photocatalytic degradation of the MB aqueous solution catalyzed by the TNAs powders prepared at different conditions. a, before solvothermal process; b, 80 °C for 3 h; c, 100 °C for 3 h; d, 120 °C for 3 h; e, 150 °C for 3 h; (B) Successive UV–vis spectra of the MB photocatalytic degradation in the presence of the TNAs powders prepared via solvothermal treatment at 150 °C for 3 h.. The concentration of the reactants is [MO]=20 mg/L and [photocatalysts]=0.1 g/L.

3.6. Photocatalytic activity analysis

Photocatalytic activities of the samples were evaluated by a decomposition of the MB aqueous solution under UV and visible light irradiation. In order to study the influence of the solvothermal treatment on the photocatalytic activities, the TNAs powders photocatalysts obtained at different reaction temperatures were used to decompose the MB aqueous solution. Fig. 7A shows that the TNAs powders before solvothermal process have little photocatalytic activities, only about 18 % of the MB aqueous solution can be decomposed after 180 min, while the TNAs powders after solvothermal treatment exhibit an enhanced photocatalytic activity. Especially, the TNAs powders after solvothermal treatment at 100 °C for 3 h show the best photocatalytic activity among all the samples, and the kinetics of this reaction was monitored by UV–vis spectroscopy as seen from UV–vis spectra measured at different time shown in Fig. 7B. These results indicate that the MB shows a strong absorption band at 665 nm and the addition of the TNAs powders leads to a decrease of the absorption band with time. There are many reasons that affect the photocatalytic activity, such as anatase crystallinity, N-doping, introduction of the disorder, and nitride species on the surface or in pores which play an important part in the photocatalysis process. These nitride species can act as an active site and

thus enhance the reaction during the photocatalysis process. In addition, anatase crystalline also can enhance the activity by reducing the electron–hole recombination [30,31]. In short, the TNAs powders with proper crystalinity after solvothermal process at 100 °C for 3 h can balance the formation and recombination of the electron–hole pair.

4. Conclusions

In this study, we have demonstrated that the N-TNAs powders can be easily prepared by a two-step process, which combines the anodization method with the solvothermal treatment process. After the solvothermal treatment, the N-TNAs powders transform amorphous to anatase phase and the surface of N-TNAs is covered by many nanoparticles. Results also indicate that the electrochemical properties of these TNAs powders show good reversible capacity and the TNAs powders after solvothermal treatment at 100 °C for 3 h have the best photocatalytic activities among all the measured samples due to proper crystalinity, which is helpful for balancing the formation and the recombination of the electron–hole pair.

Acknowledgments

This work was supported by the Major Program of the National Natural Science Foundation of China (Nos. 90923012 and 61078058), The Research Fund for the Doctoral Program of Higher Education of China (20120201130004), and the Science and Technology Developing Project of Shaanxi Province (No. 2012KW-11).

References

[1] M.N. Ańamt, S. Radiman, N.M. Huang, M.A. Yarmo, N.P. Ariyanto, H.N. Lim, M.R. Muhamad, Sol–gel hydrothermal synthesis of bismuth–TiO_2 nanocubes for dye-sensitized solar cell, Ceramics International 36 (2010) 2215–2220.

[2] H.G. Bang, J.K. Chung, R.Y. Jung, S.Y. Park, Effect of acetic acid in TiO_2 paste on the performance of dye-sensitized solar cells, Ceramics International 38 (2012) S511–S515.

[3] E.C. Muniz, M.S. Góes, J.J. Silva, J.A. Varela, E. Joanni, R. Parra, P.R. Bueno, Synthesis and characterization of mesoporous TiO_2 nanostructured films prepared by a modified sol–gel method for application in dye solar cells, Ceramics International 37 (2011) 1017–1024.

[4] X.B. Chen, L. Liu, P.Y. Yu, S.S. Mao, Increasing solar absorption for photocatalysis with black hydrogenated titanium dioxide nanocrystals, Science 331 (2011) 746–750.

[5] H. Tian, J.F. Ma, K. Li, J.J. Li, Hydrothermal synthesis of S-doped TiO_2 nanoparticles and their photocatalytic ability for degradation of methyl orange, Ceramics International 35 (2009) 1289–1292.

[6] He Z.L. Que W.X. Chen J. Yin X.T. He Y.C. Ren J.B. Photocatalytic degradation of methyl orange over nitrogen-fluorine codoped TiO2 nanobelts prepared by solvothermal synthesis. ACS Applied Materials & Interfaces 4 (2012) 6816–6826.

[7] N. Yao, C.C. Wu, L.C. Jia, S. Han, B. Chi, J. Pu, L. Jian, Simple synthesis and characterization of mesoporous (N, S)-codoped TiO_2 with enhanced visible- light photocatalytic activity, Ceramics International 38 (2012) 1671–1675.

[8] L. Yang, P. Liu, X. Li, S. Li, The photo-catalytic activities of neodymium and fluorine doped TiO_2 nanoparticles, Ceramics International 38 (2012) 4791–4796.

[9] Z.L. He, Z.F. Zhu, J.Q. Li, N. Wei, J.Q. Zhou, Characterization and activity of mesoporous titanium dioxide beads with high surface areas and controllable pore sizes, Journal of Hazardous Materials 190 (2011) 133–139.

[10] J. Wang, D.N. Tafen, J.P. Lewis, Z.L. Hong, A. Manivannan, M.J. Zhi, M. Li, N.Q. Wu, Origin of photocatalytic activity of nitrogen-doped TiO_2 nanobelts, Journal of the American Chemical Society 131 (2009) 12290–12297.

[11] F.K. Meng, J.T. Li, Z.L. Hong, M.J. Zhi, A. Sakla, C.C. Xiang, NQ. Wu, Photocatalytic generation of hydrogen with visible-light nitrogen-doped lanthanum titanium oxides, Catalysis Today 199 (2013) 48–52.

[12] F.K. Meng, Z.L. Hong, J. Arndt, M. Li, M.J. Zhi, F. Yang, N.Q. Wu, Visible light photocatalytic activity of nitrogen-doped $La_2Ti_2O_7$ nanosheets originating from band gap narrowing, Nano Research 5 (3) (2012) 213–221.

[13] Z.L. He, W.X. Que, Y.C. He, Synthesis and characterization of bioinspired hierarchical mesoporous TiO_2 photocatalysts, Materials Letters 94 (2013) 136–139.

[14] Z.F. Zhu, J.Q. Zhou, Z.L. He, J.Q. Li, H. Liu, Preparation, characterization and activity of $TiO_{2-x}F_x$ spherical photocatalyst: influence of sodium fluoride on methyl orange degradation, Materials Research Innovations 15 (2011) 78–82.

[15] Z.L. He, W.X. Que, H.X. Xie, J. Chen, Y. Yuan, P. Sun, Facile synthesis of self-sensitized TiO_2 photocataslysts and their higher photocatalytic activity, Journal of the American Ceramic Society 95 (12) (2012) 3941–3946.

[16] Z.F. Zhu, Z.L. He, J.Q. Li, J.Q. Zhou, N. Wei, D.G. Liu, Two-step template-free route for synthesis of TiO_2 hollow spheres, Journal of Materials Science 46 (2011) 931–937.

[17] Z.L. He, W.X. Que, Y.C. He, J. Chen, H.X. Xie, G.F. Wang, Nanosphere-assembled mesoporous titanium dioxide used absorbent cotton as template and research on photocatalystic activity, Journal of Materials Science 47 (2012) 7210–7216.

[18] J.F. Yan, F. Zhou, TiO_2 nanotubes: structure optimization for solar cells, Journal of Materials Chemistry 21 (2011) 9406–9418.

[19] Z. Jiang, F. Yang, N.J. Luo, Bryan T.T. Chu, D. Sun, H.H. Shi, T.C. Xiao, Peter P. Edwards, Solvothermal synthesis of N-doped TiO_2 nanotubes for visible-light-responsive photocatalysis, Chemical Communications (2008) 6372–6374.

[20] H.L. Li, L.X. Cao, W. Liu, G. Su, B.H. Dong, Synthesis and investigation of TiO_2 nanotube arrays prepared by anodization and their photocatalytic activity, Ceramics International 38 (2012) 5791–5797.

[21] H.H. Wu, L.L. Li, C.C. Chen, E.W.G. Diau, Anodic TiO_2 nanotube arrays for dye-sensitized solar cells characterized by electrochemical impedance spectroscopy, Ceramics International 38 (2012) 6253–6266.

[22] A.W. Tan, B. Pingguan- Murphy, R. Ahmad, S.A. Akbar, Review of titania nanotubes: fabrication and cellular response, Ceramics International 38 (2012) 4421–4435.

[23] G.Q. Wu, J.W. Zhang, X.Y. Wang, J.J. Liao, H. Xia, S.A. Akbar, J.B. Li, S.W. Lin, X.G. Li, J. Wang, Hierarchical structured TiO_2 nano-tubes for formaldehyde sensing, Ceramics International 38 (2012) 6341–6347.

[24] X.Z. Wei, H.J. Wang, G.F. Zhu, J.Y. Chen, L.P. Zhu, Iron-doped TiO_2 nanotubes with high photocatalytic activity under visible light synthesized by an ultrasonic-assisted sol-hydrothermal method, Ceramics International 10 (2012), http://dx.doi.org/10.1016/j.ceramint.2012.10.251, in press.

[25] J.T. Li, F.K. Meng, S. Suri, W.Q. Ding, F.Q. Huang, N.Q. Wu, Photoelectrochemical performance enhanced by a nickel oxide–hematite p–n junction photoanode, Chemical Communications 48 (2012) 8213–8215.

[26] Scott K. Cushing, J.T. Li, F.K. Meng, Tess R. Senty, S. Suri, M.J. Zhi, M. Li, Alan D. Bristow, N.Q. Wu, Photocatalytic activity enhanced by plasmonic resonant energy transfer from metal to semiconductor, Journal of the American Chemical Society 134 (2012) 15033–15041.

[27] Z.F. Zhu, Z.L. He, J.Q. Li, D.G. Liu, N. Wei, Synthesis and characterization of fluorinated TiO_2 microspheres with novel structure by sonochemical-microwave hydrothermal treatment, Materials Research Innovations 14 (2010) 426–430.

[28] R. Asahi, T. Morikawa, T. Ohwaki, K. Aoki, Y. Taga, Visible-light photocatalysis in nitrogen-doped titanium oxides, Science 293 (2001) 269–271.

[29] M.C. Wang, H.J. Lin, C.H. Wang, H.C. Wu, Effects of annealing temperature on the photocatalytic activity of N-doped TiO_2 thin films, Ceramics International 38 (2012) 195–200.

[30] Z.L. He, W.X. Que, Enhanced photocatalytic activity of N-Cetyl-N,N,N-Trimethyl ammonium bromide-assisted solvothermal grown fluff-like ZnO nanoparticles, Journal of Nanoengineering and Nanomanufacturing 2 (2012) 17–21.

[31] Z.F. Zhu, J.Q. Zhou, Z.L. He, J.Q. Li, H. Liu, Synthesis and visible light photocatalytic activity of Mo–N codoped TiO_2 nanowires prepared by amorphous titania spheres via hydrothermal process, Materials Research Innovations 15 (2011) 254–259.